CHAPTER IV
RESULTS AND DISCUSSION

4.1 Catalyst Characterization

4.1.1 Elemental Analyses by XRF

Table 4.1 Elemental analysis of the catalysts synthesized

Catalyst	Composition (wt%)			
	Ce	Zr	Ni	O
$Ce_{0.75}Zr_{0.25}O_2$	67.29	12.71	-	20.00
15Ni/ $Ce_{0.75}Zr_{0.25}O_2$	51.31	9.65	18.52	20.52

Table 4.1 shows the chemical compositions obtained from XRF analyses, expressed as weight percentages, of the investigated catalysts. The composition of $Ce_{0.75}Zr_{0.25}O_2$ support is closely to mol percent of Ce=0.75 and Zr=0.25 and for 15wt% Ni/$Ce_{0.75}Zr_{0.25}O_2$ weight percent of Ni is close to 15% so the catalyst use in this research is close to 15wt% Ni/$Ce_{0.75}Zr_{0.25}O_2$.

4.1.2 Textural Properties of the catalysts

Table 4.2 Textural Properties

Catalyst	Surface Area (m^2/g)	Pore Volume (cm^3/g)	Average Pore Diameter(nm)
$Ce_{0.75}Zr_{0.25}O_2$	79	0.046	4.0
15wt% Ni/$Ce_{0.75}Zr_{0.25}O_2$	57	0.037	6.9

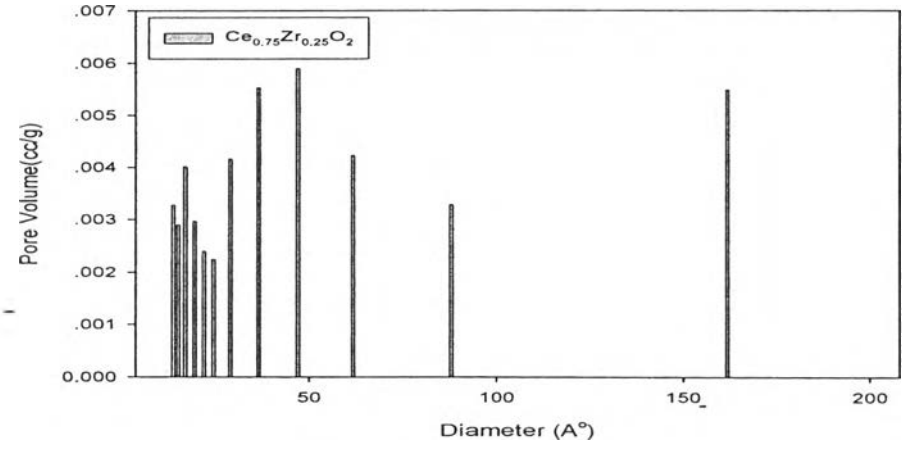

Figure 4.1 Pore size distribution of $Ce_{0.75}Zr_{0.25}O_2$.

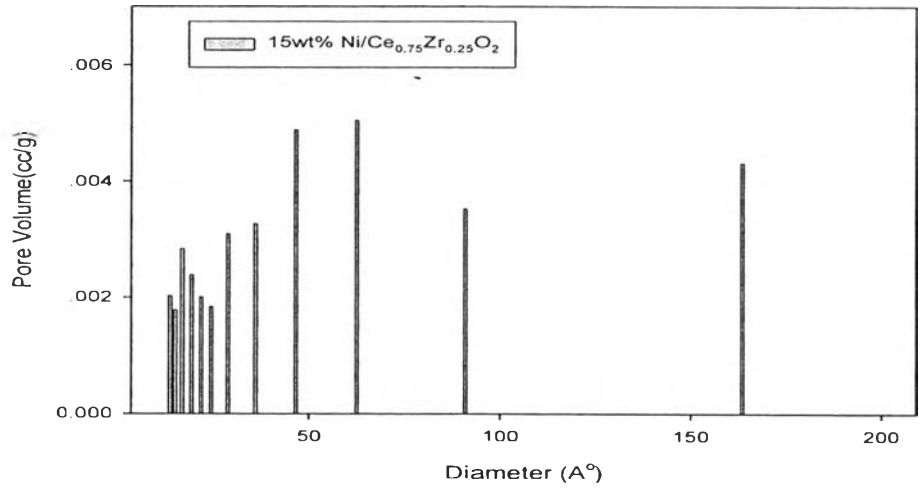

Figure 4.2 Pore size distribution of 15wt% $Ni/Ce_{0.75}Zr_{0.25}O_2$.

The surface area, pore volume and average pore diameter of the $Ce_{0.75}Zr_{0.25}O_2$ catalyst and 15wt% $Ni/Ce_{0.75}Zr_{0.25}O_2$ are depicted in Table 4.2. Both surface area of $Ce_{0.75}Zr_{0.25}O_2$ support and pore volume of $Ce_{0.75}Zr_{0.25}O_2$ support was found to decrease after impregnation with 15wt% $Ni/Ce_{0.75}Zr_{0.25}O_2$. The pore volume are $0.046cm^3/g$ and $0.037cm^3/g$ for $Ce_{0.75}Zr_{0.25}O_2$ support and 15wt% $Ni/Ce_{0.75}Zr_{0.25}O_2$, respectively as shown in Figures 4.1 and 4.2. Decrease in both total surface area and pore volume are resulted from pores blocking by the loading metal (Ni).

4.1.3 Temperature-programmed Reduction by Hydrogen (H_2-TPR)

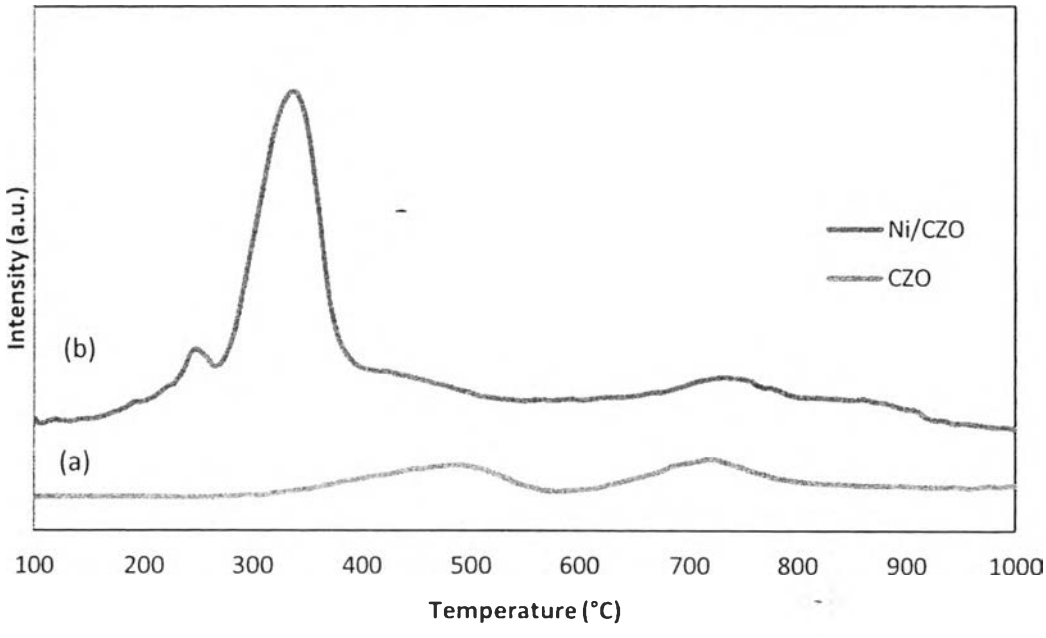

Figure 4.3 H_2-TPR profiles for the catalysts with a heating rate of 10 ◦C/min, a reducing gas containing 5% H_2 in Ar with a flow rate of 50 ml/min patterns of (a) $Ce_{0.75}Zr_{0.25}O_2$ support and (b) 15wt% $Ni/Ce_{0.75}Zr_{0.25}O_2$ catalyst.

The H_2-TPR profiles of the materials are shown in Figure 6.1 For the $Ce_{0.75}Zr_{0.25}O_2$, typical reduction peaks at 490 °C and ca. 710 °C were corresponding to a surface reduction and bulk reduction of CeO_2. For the 15wt% $Ni/Ce_{0.75}Zr_{0.25}O_2$ catalysts, the reduction peaks at 250 and 340 °C indicate the reduction of NiO to Ni^0, the lower temperature peak (250 °C) was attributed to the reduction of the relatively free NiO particles and the higher temperature one (340 °C) was attributed to the reduction of complex NiO species in intimate contact with the oxide support and the other peak was related to the bulk reduction of CeO_2 from Ce^{+4} to Ce^{+3}(Thaicharoensutcharittham *et al.*, 2009).

4.1.4 X-ray Diffraction (XRD)

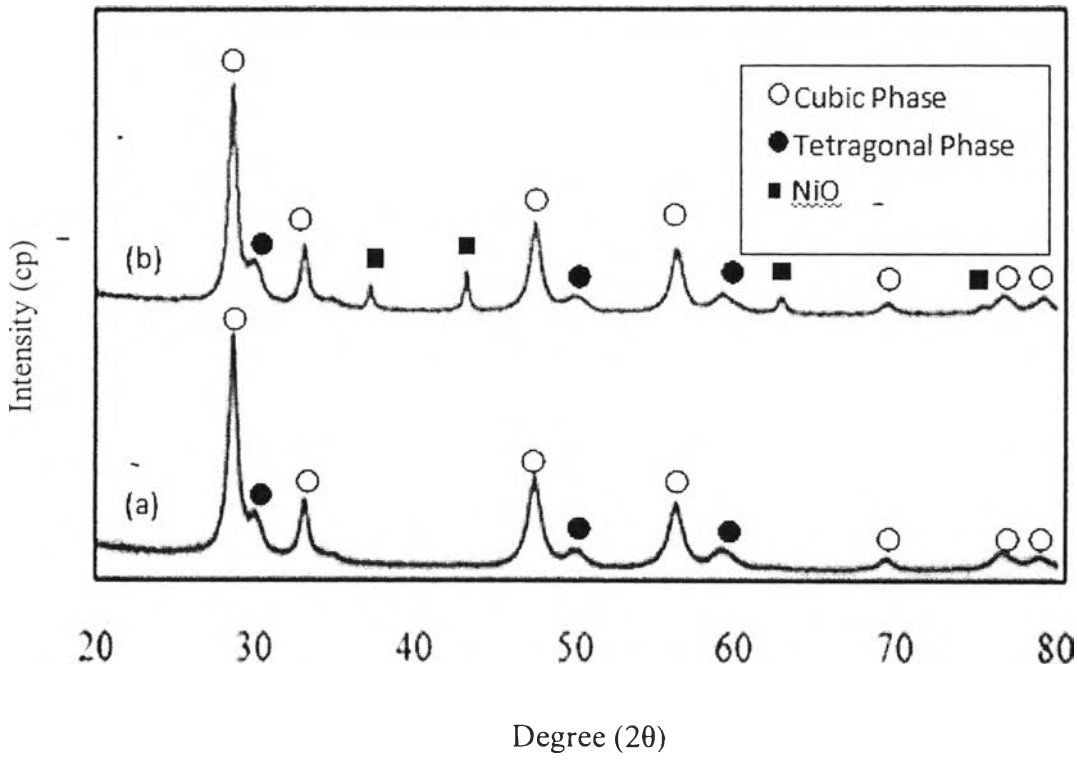

Figure 4.4 XRD patterns of (a) $Ce_{0.75}Zr_{0.25}O_2$ support and (b) 15wt% $Ni/Ce_{0.75}Zr_{0.25}O_2$ catalyst.

XRD analysis was employed to investigate the crystalline structure. The XRD patterns of $Ce_{0.75}Zr_{0.25}O_2$ support and fresh 15wt% $Ni/Ce_{0.75}Zr_{0.25}O_2$ were shown typical indices of cubic fluorite structure of CeO_2 at 28.47, 33.12, 47.51, and 56.42° (2θ), represented the plane indices of (101), (002), (112) and (103) (Pengpanich *et al.*, 2002) as seen in Figure 4.4. However, some extra peaks of tetragonal phase due to non-incorporated ZrO_2 was observed with low intensity at 30, 50.28 and 59.08° (2θ), this suggested that some of ZrO_2 cannot be incorporated in the CeO_2 lattice to form a solid solution. On the present of Ni loading indicated a typical cubic fluorite structure of ceria with the presence of NiO phase at 37.24, 43.24, 62.80 and 79.07° (2θ) represented the plane indices of (110), (111), (020) and (220) respectively.

4.1.5 Scanning Electron Microscopy (SEM)

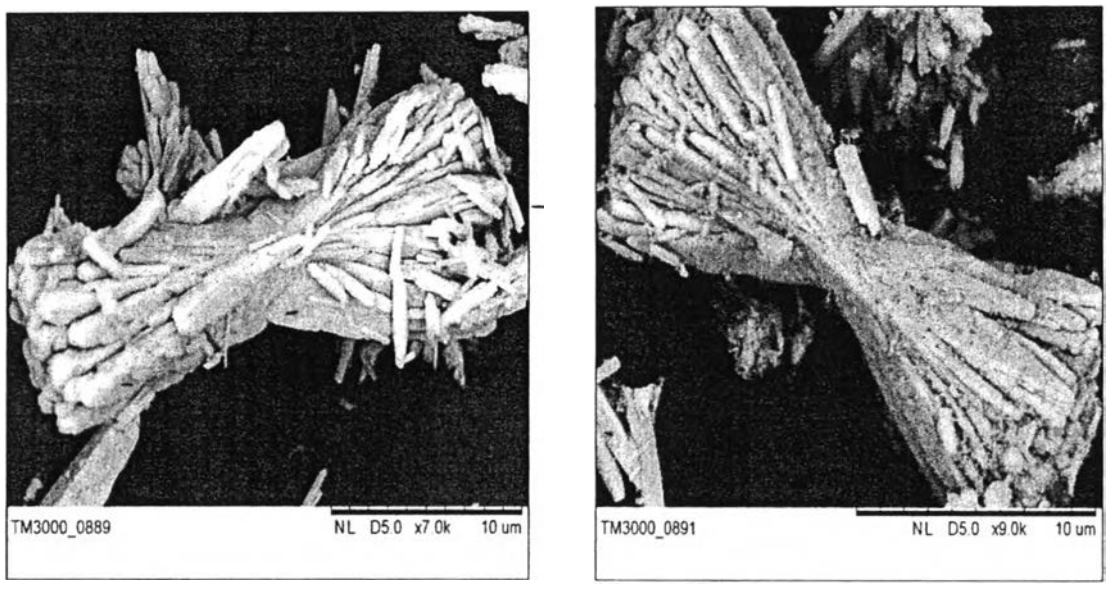

(a) (b)

Figure 4.5 SEM images of support and Ni-doped catalyst with the reflux time = 120 h, and calcined at 500°C: (a) $Ce_{0.75}Zr_{0.25}O_2$, (b) 15wt% $Ni/Ce_{0.75}Zr_{0.25}O_2$

Figure 4.5 shows SEM images of the catalysts investigated on both support ($Ce_{0.75}Zr_{0.25}O_2$) and Ni-doped catalyst (15wt% $Ni/Ce_{0.75}Zr_{0.25}O_2$) which were prepared by sol-gel technique. The aggregation of the primary long thin needle shaped particles was found in the case of zirconia-doped ceria particles (Thammachart *et al.*, 2001). For the Ni-doped catalyst, the morphology of the Ni-doped was found that the round particles of the NiO particle well distributed and attached onto the surface of long thin needle support.

4.2 Catalyst Activity Testing

Prior to the activity testing of 15wt% $Ni/Ce_{0.75}Zr_{0.25}O_2$ catalyst. The autothermal steam reforming was firstly carried out over blank tube at 650 °C, S/C ratio = 6, GHSV = 65,000 h^{-1} and O_2/AcOH = 0.34. The results showed that no products from autothermal steam reforming over blank test. The experiment data of blank test were reported in Appendix D1.

4.2.1 Effects of Temperature

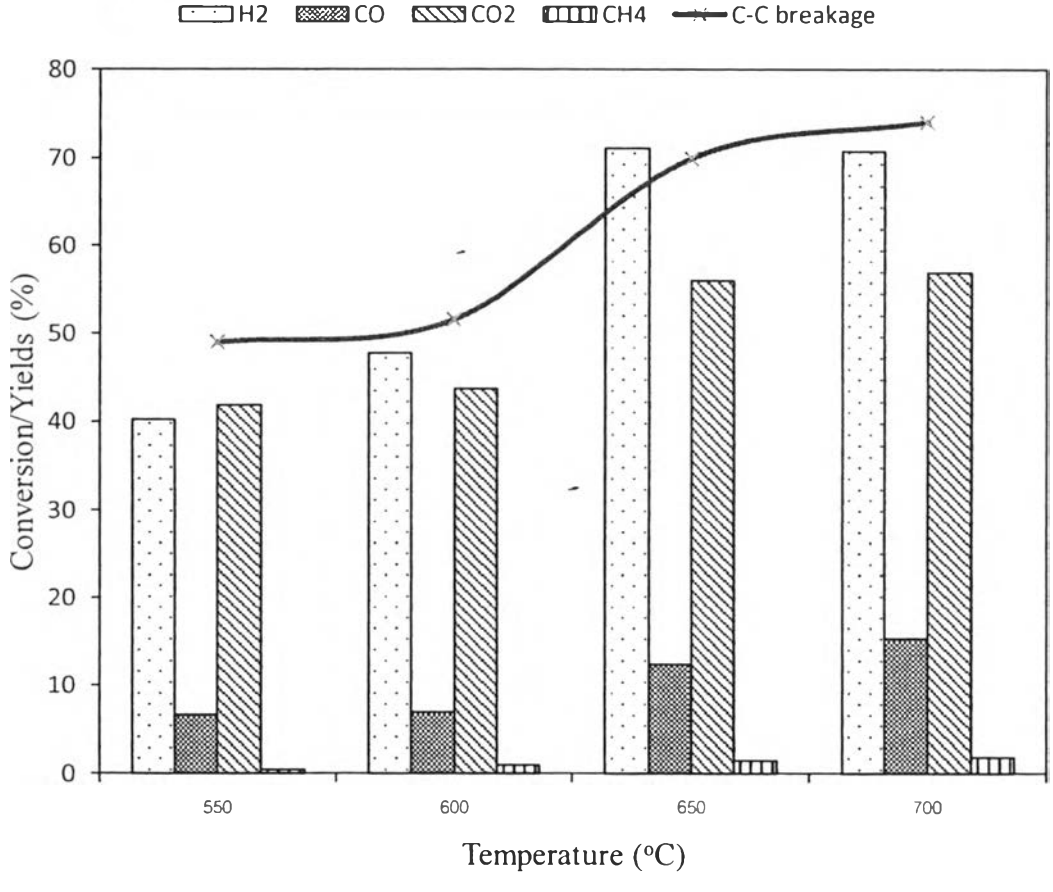

Figure 4.6 C-C breakage conversion and products distribution over 15wt% $Ni/Ce_{0.75}Zr_{0.25}O_2$ catalyst in relation to temperature, S/C = 6, ATR condition and GHSV = 65,000 h^{-1}.

The autothermal steam reforming operation is defined at a neutral condition where the endothermic steam reforming and exothermic partial oxidation are equal to achieve autothermal condition. The amount of oxygen to acetic acid molar ratio at steam-to-carbon =6 which use in temperature of 550, 600, 650 and 700 °C are 0.28, 0.30, 0.34, and 0.35, to satisfy autothermal condition. The main products in the autothermal steam reforming of acetic acid are hydrogen, carbon dioxide, carbon monoxide and methane as shown in Figure 4.6. The autothermal steam reforming products yields are increased with increasing temperature due to steam reforming reaction and decreased after temperature ca. 700°C are as a result of RWGS reaction and/or oxidation of hydrogen products. The maximum yield of hydrogen was obtained at temperature about 650 °C. Beyond this temperature, the ratio of H_2/CO started to decrease because of energetics for the reverse water-gas shift reaction. This was conformed to the thermodynamic analysis of hydrogen production via autothermal steam reforming of acetic acid and gave the highest activity at temperature around 627 °C (Ekaterini *et al.*, 2008). This temperature is still lower than that of C_2H_5OH (ca. 685°C) due to the WGS reaction (Daniel *et al.*, 2011). The C-C bond breakage conversion is increasing with temperature due to decomposition reaction.

4.2.2 Effects of Oxygen

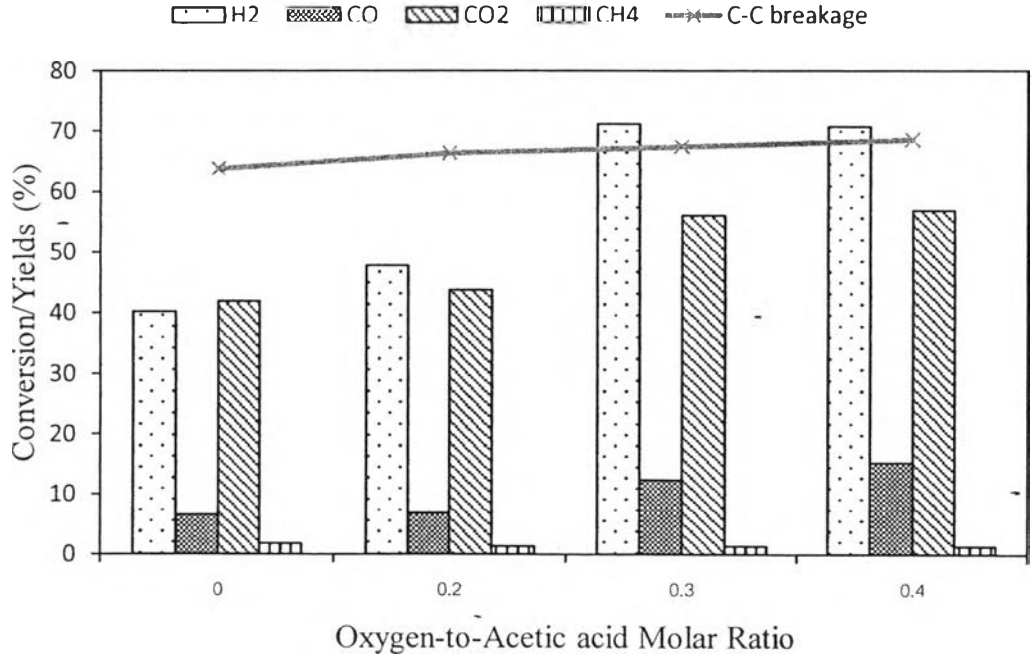

Figure 4.7 C-C breakage conversion and products distribution over 15wt% $Ni/Ce_{0.75}Zr_{0.25}O_2$ catalysts in relation to oxygen-to-acetic acid molar ratio, S/C=6, T=650°C and GHSV = 65,000 h^{-1}.

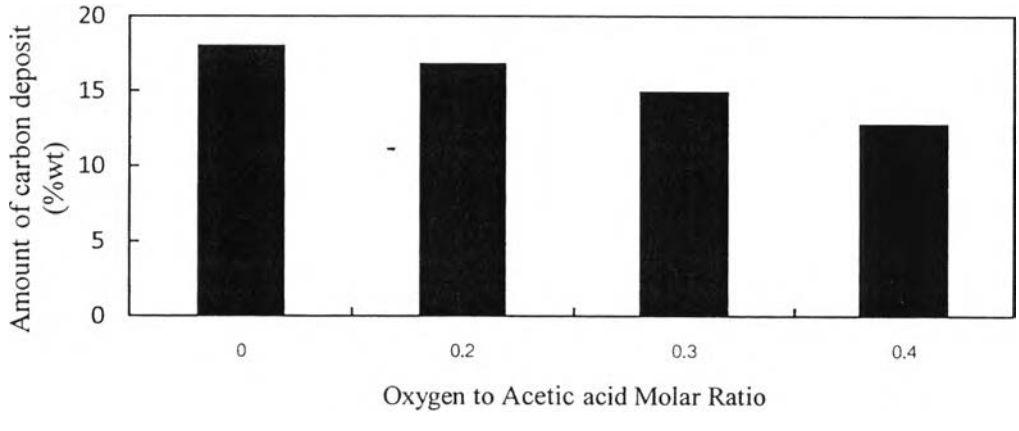

Figure 4.8 Total amount of carbon deposited on 15wt%$Ni/Ce_{0.75}Zr_{0.25}O_2$catalysts in relation to oxygen-to-acetic acid molar ratio, T=650°C, TOS = 3h, S/C=6 and GHSV = 65,000 h^{-1}.

The effects of oxygen to acetic acid molar ratio was study at 650°C steam-to-carbon=6, oxygen-to-acetic acid molar ratio to reach thermo neutral condition was at 0.34.and GHSV = 65,000 h^{-1} as shown in Figure 4.7. The results showed the C-C bond breakage conversion was increased with increasing oxygen concentration, which is along with CO_2 yield. On the other hand, the H_2 and CO yields were found to decrease with increasing O_2. Moreover, increasing oxygen partial pressure can reduce the carbon formation as showed in Figure 4.8 due to suppression of boudouard reaction. Similar finding was reported on other hydrocarbon (C16) (Shekhaeat *et al.*, 2006) and methanol (Wang *et al.*, 2009).

4.2.3 Effects of Steam

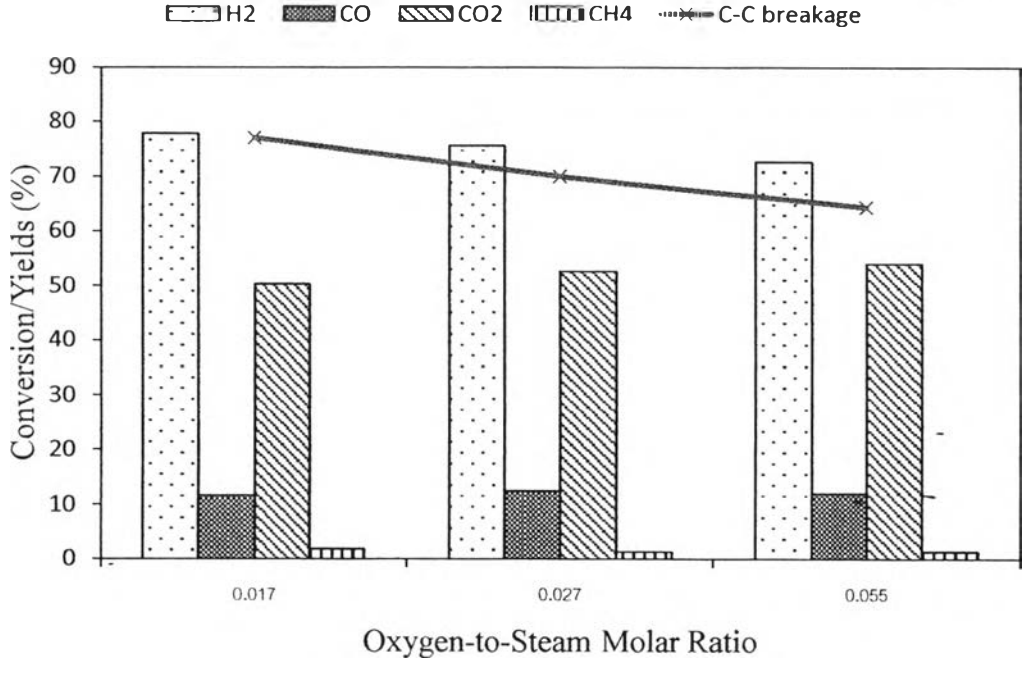

Figure 4.9 C-C breakage conversion and products distribution over 15wt% $Ni/Ce_{0.75}Zr_{0.25}O_2$catalysts in relation to oxygen-to-steam molar ratio, 650°C, ATR condition and GHSV = 65,000 h^{-1}.

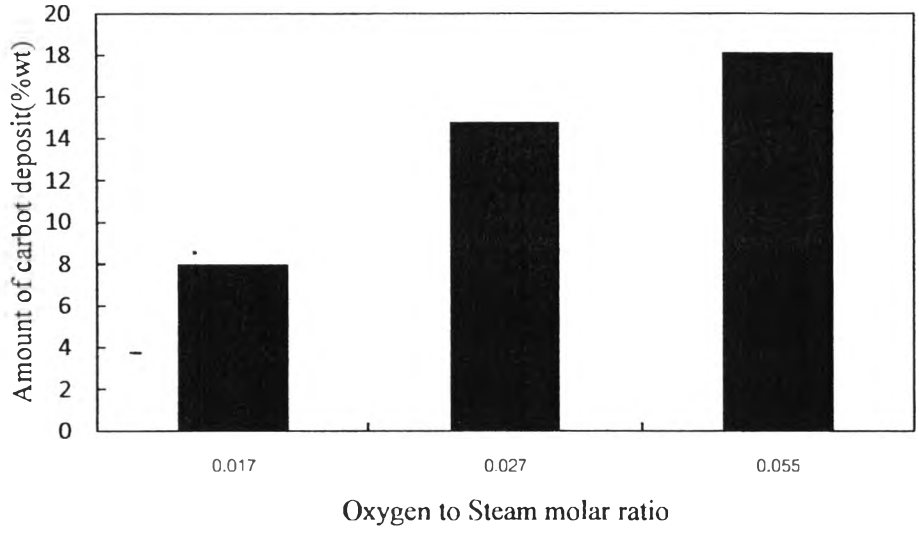

Figure 4.10 Total amount of carbon deposited on $Ni/Ce_{0.75}Zr_{0.25}O_2$ 15wt%catalyst in relation to oxygen-to-steam molar ratio, TOS = 3h, 650°C, ATR conditions and GHSV = 65,000 h^{-1}.

The effects of steam in autothermal steam reforming of acetic acid was carried out at 650°C by varying amount of steam 3-9 and fix amount of oxygen at oxygen-to-acetic acid molar ratio equal to 0.34, to yield oxygen to steam ratio from 0.017-0.055 which is equivalent to steam-to-carbon molar ratio equal to 9, 6, and 3. The temperature used in this testing is 650°C due to maximum hydrogen yield. The results on effect of oxygen-to-steam molar ratio in autothermal steam reforming of acetic acid were shown in Figure 4.9. It is apparent that by increasing oxygen-to-steam molar ratio resulted in decreasing both the H_2 and CO_2 yields but increasing CO yield due to the WGS reaction. The C-C breakage conversion was found to decrease with increasing oxygen-to-steam molar ratio, implying that cracking reactions could prevail as the oxygen-to-steam molar ratio was declined. For the carbon deposition as shown in Figure 4.10, decreasing on oxygen-to-steam molar ratio relate to increasing steam. This also retard carbon formation due to less CO resulted from WGS reaction.

4.3 Catalyst Stability Testing

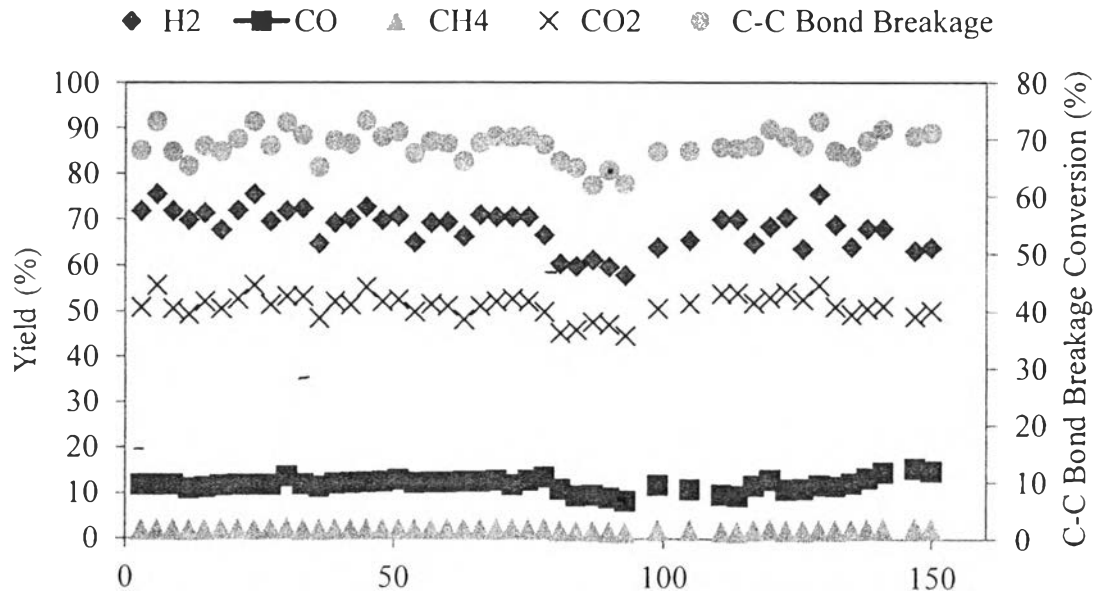

Figure 4.11 Product distribution from autothermal steam reforming stability test for 150 h, S/C=6, ATR conditions and GHSV = 65,000 h^{-1}.

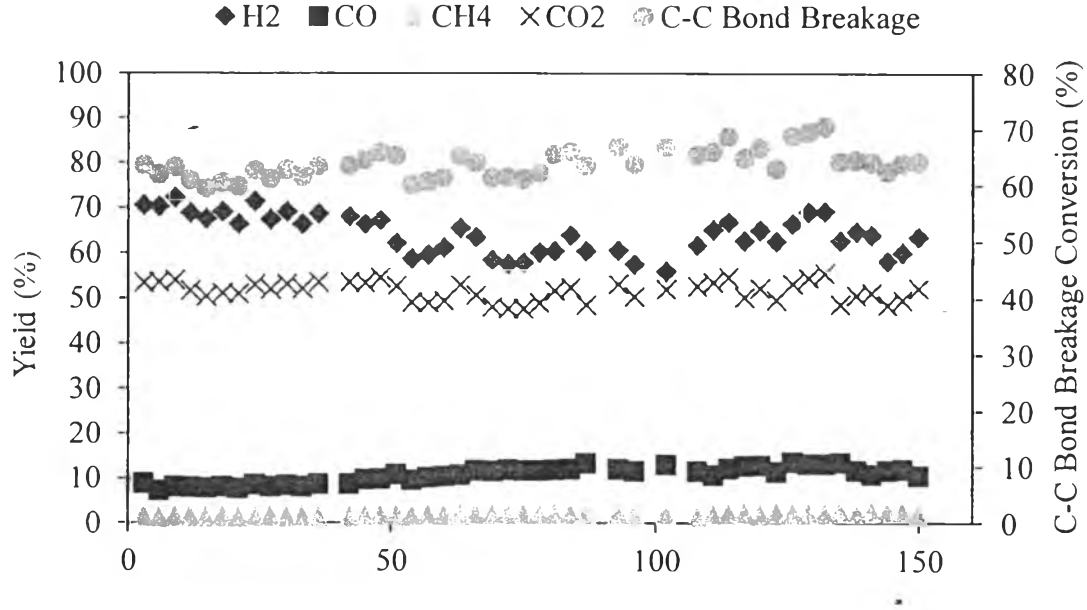

Figure 4.12 Product distribution from steam reforming stability test for 150 h, S/C=6, and GHSV = 65,000 h^{-1}.

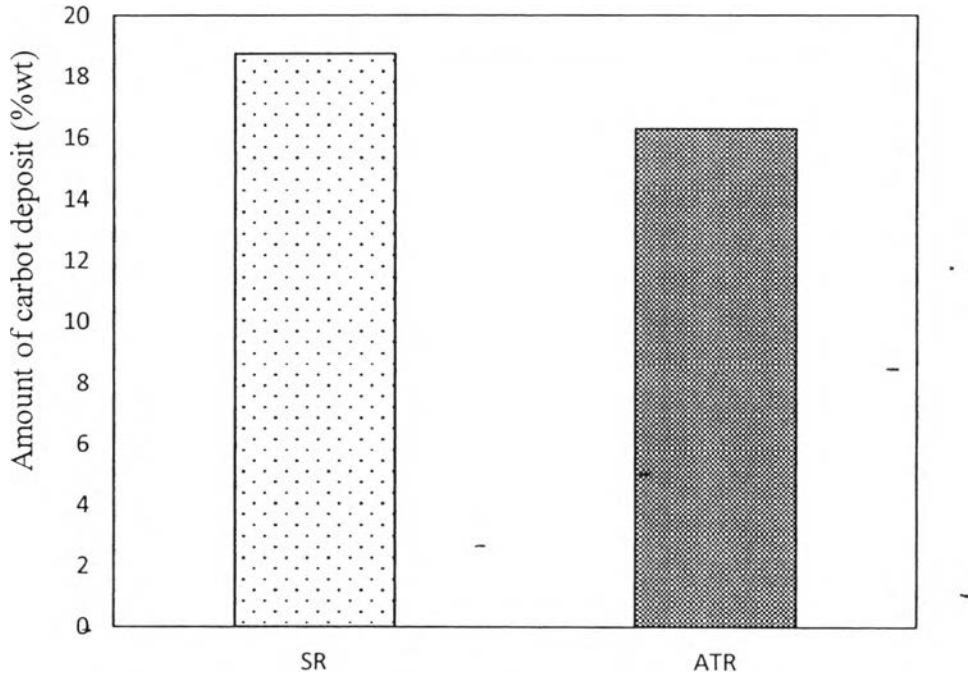

Figure 4.13 Total amount of carbon deposited on catalysts via stability testing on steam reforming and autothermal steam reforming at 150 h, S/C=6, and GHSV = 65,000 h^{-1}.

The catalyst stability was observed at 650 °C, S/C=6 and O_2/AcOH=0.34 for 150 hours on both autothermal steam reforming reaction and steam reforming reaction of acetic acid over 15wt%Ni/$Ce_{0.75}Zr_{0.25}O_2$. The results showed that autothermal steam reforming reaction and steam reforming reaction exhibited similar deactivation trends. The C-C bond breakage conversion after 150 hours on autothermal steam reforming was ca.67% and steam reforming was ca.68% which was quite stable along stability testing as depicted in Figures 4.11 and 4.12. The H_2 yield is decreased ca.7% on autothermal steam reforming and ca.8% on steam reforming. CH_4 yield were found to quite stable on both steam reforming and autothermal steam reforming, CO yield was slightly lower on autothermal steam reforming than steam reforming and CO_2 yield of autothermal steam reforming was slightly higher than steam reforming due to oxidation reaction. The tested catalyst was quantified for carbon formation as depicted in Figure 4.13. On both autothermal

steam reforming and steam reforming, the carbon deposition was low due to the synergetic effects of an ease of reducibility and a good oxidation ability of the $Ce_{0.75}Zr_{0.25}O_2$ mixed oxide which promote the oxidation of carbon precursors on the nickel surface (Thaicharoensutcharittham *et al.*, 2009). The carbon formation of autothermal steam reforming was slightly lower than steam reforming due to less CO and suppression of boudouard reaction.